SELF-REFERENCING GUIDANCE INTERFEROMETER

FINAL REPORT

by

G. Tricoles
R.A. Hayward
E.L. Rope

Prepared for

U.S. Naval Air Systems Command

Contract N00019-79-C-0637

GENERAL DYNAMICS

CONTENTS

ii

ILLUSTRATIONS

ILLUSTRATIONS

(Continued)

SUMMARY

This report describes the results of a seven month study of a new
approach to direction finding and missile guidance. The approach
combines the functions of an antenna and a radome. The essential
physical concept is that a wave incident on a dielectric slab excites
two kinds of waves. One kind is approximately plane refracted,
reflected, and transmitted waves. The other kind is guided. These
two kinds of waves have distinct propagation constants, but they
interfere to form fringes if the incident wave has sufficient
coherence length. We have found magnetrons have sufficient coherence.
The name self-referencing comes from the generation of two coherent
waves by an incident coherent waves.

The fringe pattern is useful for direction finding because δs the
separation of intensity minima depends on incidence angle α according
to the relation that

$$\delta s = 2\,\pi\,(k_g - k_o\,\sin\alpha)^{-1}$$

where k_g is the propagation constant of the slab and k_o is the pro-
pagation constant in free space. In addition to spacing incidence
angle affects the position of fringes. Both δs and fringe position
can be sensed for direction finding.

This report describes three approaches to direction finding. One
uses a sampling array to determine fringe spacing. Another utilizes
only two antennas to sense shifts in fringe position. The third
utilizes two interferometers in the form of a wedge to form monopulse
type patterns.

The work was based on numerical values of fields in slabs. Cal-
culations were based on the moment method. Farfield patterns
also were computed. Experiments verified the computed nearfield
and farfield values.

The gain of a single dipole in a slab was measured as 10 1/4 dBi
and the gain of a dipole on the slab surface was 12 dBi. For two
dipoles in a wedge we expect gain values between 13 and 15 dBi.
These are practical values. The gain was greater for tapered die-
lectric thickness than for uniform slabs.

Sidelobe levels of a single antenna in a slab were reduced by
metallic foil and wires. The latter acted as directors and re-
flectors.

The direction of wave polarization was found significant. The reason
is that k_g for parallel polarization differs from k_g for perpendi-
cular. This difference is a factor in planning a system because it
influences antenna orientation. The question of polarization re-
flects the strong influence that applications or missions place on
interferometer configuration.

The final section of the report gives an assessment of technical
factors that influence further research and development. Problems
and approaches to solution are given.

1. INTRODUCTION

1.1 The concept of a Self-Referencing Interferometer

The term self-referencing interferometer describes a finite dielectric slab with sensors such as dipole antennas connected to detectors. More general structures are possible. For example, the dielectric can be a hollow shell, and the sensors might be antennas. However, flat dielectrics emphasize the physical basis. The essence of this interferometer is that an incident wave excites two coherent waves that have distinct propagation constants.*

Figure 1 suggests these waves.** An incident wave generates reflected and refracted waves in the slab, a transmitted wave on the shadowed side, and a reflected wave on the illuminated side. In addition a guided wave propagates parallel to the slab. The guided wave exists within and outside the slab. On the outside, the amplitude decreases exponentially with distance from the slab plane. The guided wave has propagation constant k_g different from k_o, for the incident and transmitted waves, and from $\sqrt{\kappa}\, k_o$ the propagation constant of the internal waves, where κ is dielectric constant. The value of k_g can be determined with reasonable accuracy from solutions of a boundary value problem.[1]*** The mathematical procedure is outlined in Reference 1, and some examples are given in Reference 2.

The slab-guided wave and the transmitted wave interfere to form intensity fringes, as suggested in Figure 2. Fringe spacing δs is a convenient quantity for testing the conceptual model in Figure 1. To describe fringe spacing, assume an incident wave with amplitude proportional to $\exp(ik_o s \sin\alpha)$ and let the guided wave amplitude be proportional to $\exp ik_g s$, where s is the distance from the slab edge that is nearer the wave source and d is incidence angle. Fringe spacing δs is the distance such that the phase difference between the two waves changes by 2π; that is,

$$2\pi = \delta s (k_g - k_o \sin\alpha). \tag{1}$$

*The term self-referencing emphasizes the local generation of two waves that interfere. We do not imply that either wave is a reference wave or object wave as those terms are used in holography.

**We have assumed the source to be in the plane of Figure 1. Skew incidence is considered in another section.

***References are collected in Section 6.

1

This formula has been verified by experiment and by moment method calculations.[2,3] Measurement of δs, together with the values of k_g and k_o determines α and thus source direction. Equation 1 also describes fringe spacing within the slab, this result follows by applying Snell's law, but we omit the proof for brevity.

The physical model underlying Equation 1 is approximate because it omits higher order guided modes and a guided wave that is reflected toward the right side of Figure 1. The reflected guided wave has small amplitude so it produces shallow ripples on the fringe pattern.[4] The ripples can be virtually eliminated by tapering the slab edge that is farther from the source. Higher order modes can be eliminated by choosing slab thickness. The slab must be long enough to justify assuming plane internal waves and a slab guided wave.

The model does not give guided wave amplitudes, but the moment method does.[5] By postulating guided waves of the form $A \exp i k_g s$ and $B \exp(-i k_g s)$, A and B can be determined from moment method calculations for fields in slabs. Figure 3 shows A . In all cases B was less than 0.3 for unit incident wave amplitude.

1.2 Interferometer Configurations and Data Acquisition

This section describes methods for extracting angle information from the fields on slabs. It presents three configurations to describe what can be measured, the measurement means, and the data that are obtained. Again direction is determined in one plane; a subsequent section considers three dimensions.

1.2.1 Interference Fringe Spacing for a Slab.

Equation 1 determines direction from measured values of δs. Although laboratory measurements can be made by moving a probe through the fringe pattern, the time delay and complexity of mechanical scanning are unsuitable for applications such as missile guidance or direction finding. Therefore, a sampling array like that in Figure 4 seems necessary. Each dipole is connected to an intensity detector; a corporate feed is not used. Figure 5 shows measured and computed fringe spacings. Although the array uses simple components, it has disadvantages. First, field amplitude is small near fringe minima so noise can obscure their locations; however, the field amplitude can be increased by tapering slab thickness.* Second, the antennas must be closely spaced to adequately sample the fringe pattern; scattering by the elements will distort the fringe pattern. Third, the fringe spacing varies with position because the edges of the slab scatter the waves.

In Figure 5, the vertical spread in δs values for a fixed incidence angle illustrates the variation with position along the slab. The spread in δs produces an error in α. To assess the error magnitude we measured δs for typical cases with the array in Figure 4. Figure 6 shows an example. Two values of δs were determined from three adjacent minima. The two values of δs were averaged to determine α. The difference between the time value and that from the averaged δs was 0.16°. This error is acceptable boresight error in current missile radomes.

*Data are given in Section 3.

3

1.2.2 Positions of Interference Minima

The positions of fringe minima depend on incidence angle. Figure 7 shows an approximately linear relationship. This property can be utilized by placing two antennas on a slab. The antenna would straddle a minimum in the fringe pattern for a specific incidence angle value α_o. The fields received by the two antennas would be approximately equal, and subtraction would produce a minimum. For α different from α_o, the magnitude of the field difference would increase as α departs from α_o. Figure 8 shows computed values of the difference in field magnitudes for a slab and perpendicular polarization.

This approach requires fewer antennas than does the array in Figure 4. The two antennas could be connected to a hybrid junction for coherent detection, or two, separate intensity detectors can be used. Coherent detection would give higher signal levels. This approach has the further advantage that the antennas (or other sensors) are located near maxima. These signals are higher than those near minima which are sensed by the array in Figure 4.

1.2.3 Monopulse Type, Sum and Difference Patterns from a Hollow Wedge

A hollow wedge, composed of two slabs, each with a dipole, can be utilized to form monopulse type patterns, with either a minimum or a maximum on the symmetry plane. The antennas are connected to a hybrid junction, which sums their amplitudes before detection. Alternatively, the detected intensities on the opposite sides of the wedge can be compared. Coherent addition in a hybrid gives greater intensity than power addition.

Some measured patterns are presented in Section 3.

4

1.3 Gain

The gain G is a significant parameter for antennas. In a receiving
system the power received is proportional to G so that G influences
detection range. Typical values of G for missile seekers are 16 dB
to 22 dB above the isotropic level.

For a self-referencing interferometer a value of G can be determined,
but the value depends on the sensor that extracts energy. Clearly,
the gain depends on the field amplitude at the sensor. Field amplitude
depends on incidence angle and location along the slab. In Figure 3
the guided wave amplitude approaches 2 for unit incident amplitude.
Where the guided wave and the other waves add, the amplitude can be
as large as 3 so that power density can be as much as 9 1/2 dB above
that in the incident wave. If a half-wave dipole sensor were used,
the gain would be approximately 11 1/2 dBi.

The gain for a wedge composed of two slabs, each with a dipole, would
be approximately 14 dB if the antennas were connected into a hybrid
junction. Gain can be further increased approximately 3 dB by uti-
lizing two colinear dipoles on each slab.

1.4 Antenna Patterns

The radiation patterns of an antenna near a slab will differ from
those of the antenna in free space. The difference arises because
the total field at the antenna location depends on the angle of in-
cidence in the slab. The antenna might be external, like those in
Figure 4, or embedded as Figure 9. Although measured patterns are
somewhat specialized by the choice of a specific antenna, the
patterns have some value. The results can be compared with numerical
results. Moreover, the patterns can help develop more general sensors by
providing quantitative data on field variation with incidence angle.

A subsequent section gives measured antenna patterns for dipole
antennas in two slab configurations and in a wedge.

5

2.   CALCULATION

This section describes calculations of field intensities produced in flat, finite slabs by incident plane waves. The calculations are made by the moment method so this section briefly describes the method. Two examples are given. One is a uniform slab; the other has tapered thickness. The intensities are shown first as a function of position for a fixed incidence angle. This spatial distribution serves to locate elementary sensors along the slab for maximum gain. The intensities also are shown as functions of incidence angle for fixed position in the slab. These angular distributions approximate the farfield radiation patterns of antennas embedded in slabs.

2.1   The Moment Method

The moment method is a mathematical procedure for solving scattering and diffraction problems. In this method the scattered field is described by an integral equation, and the integral equation is changed to a set of simultaneous algebraic equations. The scatterer is represented by a set of simpler scatterers, called cells. For example, Figure 10 shows how a hollow wedge (or a hollow cylinder) can be represented by a set of cylinders with infinite lenghts; for this subdivision, the incident wave normal is orthogonal to the cylinder axis. The purpose of the subdivision is to justify assuming that the field in any one cylinder is constant. This assumption requires the cylinders to have radius considerably smaller than the wavelength. It justifies removing the unknown total field E^T from under the integral sign and thus simplifies evaluating integrals, which appear as known co-efficients in the integral equation.

The integral equation gives the scattered field as

$$E^S = (\kappa - 1)(4\pi)^{-1} \int E^T g \, dV \tag{1}$$

6

where κ is dielectric constant (assumed constant in the scatterer for convenience of this description) and g is r^{-1} expikr, with r the distance between integration and observation points. The subdivision into cells gives

$$E_m^S = (\kappa-1)(4\pi)^{-1} \sum_{n=1}^{N} E_n^T C_{mn} g dV, \qquad (2)$$

where E_n is the total field in the cell labelled with index n. Equation 2 is evaluated at the center of each cell. These values of E^I are labelled with index m, which takes the N values, $1 \leq m \leq N$; thus

$$E_m^S = (\kappa-1)(4\pi)^{-1} \sum_{n=1}^{N} E_n^T C_{mn}$$

where the

$$C_{mn} = \int g dV$$

where r is now $r_{mn} = [(x_m - x)^2 + (y_m - y)^2 + (z_m - z)^2]^{1/2}$, (x_m, y_m, z_m) are co-ordinates at the center of the cell labelled with index m and (x, y, z) are integration co-ordinates.

The magnitudes of the guided waves were determined approximately by assuming the internal field has the from

$$E^T = Ae^{ik_g x} + Be^{-ik_g x} + (T + R)e^{ik_x x}$$

where k_x is $k_o \cos\phi_i$, with k_o equal $2\pi/\lambda$, λ the wavelength and $\phi_i = (\pi/2) - \alpha$.

7

2.2 Calculations for a Uniform Slab

Figure 11 shows computed values of $|E^T|^2$ for a finite slab with uniform thickness and for the incidence angle 45°. The fringe spacings agree well with those from Equation 1. Calculations were made for additional angles but they are omitted for brevity. These calculations show that $|E^T|^2$ has maxima for all incidence angles in a region centered near $x = 6$ cm in Figure 9.

The regions in which $|E^T|^2$ is largest seem suitable for the positions of antennas (or other sensors). We would expect to obtain the largest gain from an antenna placed where $|E^T|^2$ is greatest. Of course a reasonably accurate calculation of the variation of $|E^T|^2$ with incidence angle is necessary to evaluate the properties of an embedded antenna or the response of any sensor.

Figure 12 shows $|E^T|^2$ for a single slab, at the position $X = 6.3$ cm, as a function of angle ϕ_i. Figure 13 shows $|E^T|^2$ produced by combining the E^T values for two positions.

The graphs of $|E^T|^2$ are equivalent to antenna patterns. They are approximate because scattering by embedded antennas is omitted, moreover the gain of embedded antenna is absent in the values of $|E^T|^2$. The computed values in Figures 12 and 13 are normalized to the incident field intensity.

Neither pattern (Figure 12 nor 13) is practical because the sidelobe levels are high. The value of these computed patterns is for comparison with measurement to evaluate the assumptions on antenna scattering are to verify normalization.

8

2.3 Tapered Slab

We tapered a slab to reduce sidelobe levels, to increase beam collimation, and to tilt the beam spproximately 20° above the slab plane. This tilt anticipates two slabs formed into a wedge. The tilt would put the beam maximum on the wedge symmetry axis. This orientation is desireable because it corresponds approximately to the flight direction of an airplane or missile.

Figure 14 shows the configuration of the slab, and Figure 15 shows the computed values of $|E^T|^2$ as a function of angle. Although Figure 14 shows metallic foil and wires that help shape the pattern, the calculation omitted the foil, which was utilized in experiments that are described in Section 3. Wires were simulated in calculations by small cylinders with κ equal 100.

3. MEASUREMENT

This section describes measured farfield patterns for four configurations. One is a dipole embedded in a uniform slab. Another is a dipole in a tapered slab. The third consists of two tapered slabs with a dipole in each. The fourth also is the wedge but it has two colinear dipoles in each tapered slab.

3.1 Uniform Slab

Figure 11 shows a measured H-plane, farfield pattern for a single half-wave dipole in a uniform slab. The pattern is normalized at $\emptyset_i = 0°$ to the measured gain of a half-wave dipole in free space. The free space dipole and the embedded dipole were tuned for maximum received power. If we assume 2 dBi gain for the half-wave dipole, the gain of the embedded dipole is 3 dBi.

9

3.2 Tapered Slab

Figure 16 shows a measured farfield pattern for a half-wave dipole embedded in the slab with tapered thickness. The slab configuration is given in Figure 14 and computed values of $|E^T|^2$ are in Figure 15. The slab had metal foil and metallic wires to reduce sidelobes below those in Figure 15.

Gain measurements also were made. The method was by comparison to a standard gain horn. For the embedded dipole, gain was 10 1/4 dBi $\pm$ 1/4 dB after the measured power level was corrected for 2 dB losses in the co-axial cable and an adapter to waveguide. The dipole was tuned for maximum gain.

Gain also was measured with the dipole on the inner surface of the slab. The recess for the embedded dipole was filled with paraffin, which has dielectric constant 2, slightly different from the 2.6 for the slab. Gain was 12 dBi, after adding 2 dB for losses

3.3 Hollow Wedge

Figure 17 shows the H-plane pattern produced by combining fields from two dipoles. One dipole was in each of the tapered slabs that formed the wedge. The antennas were connected through co-axial cables to a hybrid junction. The difference made pattern is shown in Figure 18.

Patterns were also measured with two colinear dipoles in each slab. The sum mode pattern is shown in Figure 19. The sidelobes levels are lower than those in Figure 17.

4. DISCUSSION OF MEASUREMENTS AND CALCULATIONS

Comparison of the measured and computed patterns in Figures 12 and 13 shows that the moment method values of $|E^T|^2$ agree with measured patterns despite the absence of any description of any antenna properties. The relative intensities of the measured and computed patterns agree well when the gain of the dipole is included in the measured data.

10

The tapered slab significantly lowers sidelobe levels. This result can be seen by comparing measured patterns in Figures 11 and 16. The discrepancy between the measured pattern (Figure 16) and the computed pattern (Figure 15) exists because the metallic wires and foil were omitted from the moment method calculations. Nevertheless the calculations predict correctly the trend produced by the taper for pattern angles within 40° from grazing incidence.

The gain is 10 1/4 dBi for an embedded slab and 12 dBi for the dipole on the slab. These values are significantly above those of a dipole in free space. With well designed connectors and transmission lines we expect approximately 13 to 15 dBi gain for a pair of dipoles in a wedge. For two colinear dipoles in each slab gain would be 16 to 18 dBi; these are reasonable and practical values.

The wedge configuration produced reasonable sum and difference mode patterns. Gain was not determined because a rugged, well-matched corporate feed was beyond the scope of the project.

5.   ASSESSMENT OF TECHNICAL FACTORS

The preceding sections described initial configurations of self-referencing interferometers, some calculations, and some measurements. These results defined the physical basis of the concept. However before the concept can be described as feasible for systems applications several problems must be examined. This section assesses these problems, and it gives approaches to solutions. The discussion is rather general because specific configurations depend greatly on the application. This comment is especially pertinent to Paragraph 5.7.

5.1   Applications

The self-referencing interferometer may be useful in either airplanes or missiles for three distinct functions, which are described below.

5.1.1 Passive Direction Finding

Passive direction finding is useful for threat warning and jammer location. The installation would probably be more suitable for airplanes rather than missiles because missiles usually do not take evasive maneuvers and because they cost less than aircraft.

5.1.2 Air to Surface Missile Guidance

Missile guidance against surface targets requires lower angular accuracy
than does guidance against air targets, but bandwidths usually are larger.
This application is more complex than passive direction finding because
provision must be made for generating steering signals in real-time and
because missile guidance time constants are usually shorter than those
for aircraft.

5.1.3 Air to Air Missiles

This application requires the smallest boresight error rates of change
because the target maneuvers.   The difference between active and passive
systems is significant because the polarization varies in passive (or
semi-active) systems while the missile or illuminator roll. This variation
will be discussed farther in Paragraph 5.7.

5.2 Frequency Bandwidth

The self-referencing interferometer concept can be utilized in the
frequency range between approximately 1 GHz and approximately 100 GHz.
The lower bound will be determined by the dimensions of the vehicle be-
cause the slab length must be approximately two wavelengths for the
guided wave to be established and because thickness must be adequate
to obtain one or two fringes. The upper frequency bound will be set by
dimensions of sensors; for example, antenna feed regions limit fre-
quency-independent antennas.

The operating bandwidth will depend on the sensor. A dipole has severely
limited bandwidths, but log periodic antennas have large bandwidths.
Tolerances and feed dimensions will be a limiting factor.

12

The operating bandwidth depends on how the fringe pattern changes with frequency; slab thickness is significant.

Several techniques can be utilized to increase bandwidth. Several detectors can be placed on one slab. Thickness can be tapered. Loaded dielectrics with high values of dielectric constant can be used to reduce slab size.

5.3 Number of Interferometers

A self-referencing interferometer determines angle only in one dimension. This angle is the projection onto the plane orthogonal to the slab plane. Therefore the determination of direction to a source requires two non-coplanar interferometers. The simplest arrangement seems to be an orthogonal pair, as suggested in Figure 20b. for interferometers on a missile nose. Because the nose can shadow a source, at least three interferometers are necessary, as suggested in Figure 20c. For a guidance system with two orthogonal missile control surfaces, four interferometers would be required to provide orthogonal steering signals. If the airframe rolls continuously, only two interferometers would be necessary.

5.4 Field of View

The field of view is the angular sector about the slab plane through which the interferometer is useful; see Figure 21. The definition of field of view is somewhat arbitrary, because it depends on particular applications and the sensitivity of the receiving system. However we can estimate the field of view by considering guided wave excitation for a slab.

Figure 3 shows $|A|$ the guided wave magnitude for a particular, uniform slab. For 80° incidence, $|A|$ is approximately 1.8, for unit incident wave amplitude. If the guided wave amplitude adds to the transmitted wave with

13

assumed amplitude 0.95, the total field amplitude is 2.75, so intensity is $(2.75)^2$, or 7.56; this value represents 8.6 dB. If we add 2.2 dB gain for an antenna, we expect gain to be 10.8 dB. This value agrees fairly well with the measured 12 dB value for a tapered slab.

Figure 3 also shows that $|A|$ falls to approximately 0.6 at 50° incidence. If we take the reasonable value 0.95 for the transmitted wave the total field magnitude is 1.55 so intensity is 2.4 or 3.8 dB. If we add 2.2 dB the gain is 6 dB. Thus if we take the 6 dB gain value as a minimum criterion for field of view we can obtain a field of view approximately 40° from the slab plane. If the slab is tilted 10° or 20° to the flight axis, the slab must be tapered to direct the beam onto the flight axis.

The estimate of approximately 40° is consistent with the measurements in Figure 16.

Current practical seekers have antennas that gimbal through 55° about the vehicle centerline. This range is necessary early in missile trajectories for acquisition but not for terminal guidance. In aircraft it is necessary for wide angle surveillance.

A self referencing interferometer can provide wide angle coverage by utilizing several detecting elements (such as antennas) to form a coherent array. The gain advantage over a conventional array in a radome is less than for nearly endfire, but it still exists. The array would be connected in the sum mode by switching.

5.5 Aerodynamic Heating

The wide gimbal angle of conventional seeker antennas complicates the correction of radome boresight error. The problem is especially significant at high temperatures because dielectric constant varies with longitudinal

14

position. When the seeker is gimballed, the beam encounters a non-homogeneous radome that causes refractive error. A self-referencing interferometer would greatly reduce this problem if the sensors were placed at the same station and on opposite sides of the cone. The additional temperature asymmetry produced by a small angle of attack would not be solves.

The temperature problem is significant because temperatures differ between distinct trajectories and during a trajectory. These variations complicate electronic compensation of boresight error. Such compensation could require sensors that would affect error; look up tables of measured boresight data would be large.

The self-referencing interferometer can be a dielectric slab inserted in a metal cone. In this way the slab is distant from the high temperature stagnation region. The lower temperatures would reduce the weakening of dielectrics in hypersonic flight.

5.6 Number of Sensors In a Slab Interferometer

The number of sensors in an interferometer influences performance, mainly detected field strength, angular coverage, and directional accuracy. In addition complexity and cost depend on the number of sensors. For purposes of discussion let us consider antennas. We emphasize a single slab because a wedge is similar; so is a cone if curvature is not too great.

Figure 22a shows a single sensor in a slab. A half-wave dipole has been shown earlier to provide from 10 1/2 dB to 12 dB gain. Monopulse type direction finding can be done with two slabs on cone; gain would be approximately 13 to 15 dB.

15

Figure 22b shows a slab with four sensors. This arrangement would reduce the beamwidth in the plane of the figure. It would also increase gain to approximately 16 to 18 dB for one slab. These values are reasonably high. On a cone, the gain would be approximately 19 to 21 dB for a pair of arrays. Cable losses would reduce these values somewhat, but gain approaching 20 dB seems feasible with 8 dipoles on a cone. Since 4 dipoles require a 2 wavelength baseline, four arrays would easily fit on the circumference of a missile where the diameter exceeds approximately 3 wavelengths. Additional parallel arrays could be added to increase frequency coverage.

Figure 22c shows an array of four parallel antennas. Each antenna could be connected to a detector. Alternatively each antenna could be connected through a corporate feed to sum the fields and produce a narrower beam. Phase shifters might be feasible to swing the beam, or a monopulse beam could be utilized.

5.7 Wave Polarization

The operation of a slab interferometer depends on the direction of wave polarization. The main reason is that the guided wave propagation constant k_g depends on polarization. The directions of polarization and terminology are defined in Figure 23.

Equation 1 shows that null spacing δs depends on polarization because k_g does. Some typical values of k_g for a 0.63 cm thick slab, at frequency 9.4 GHz, are 1.96 π/inch for perpendicular polarization and 1.74 π/inch for parallel. The free space propagation constant is 1.60 π/inch. For these values Equation 1 gives δs equal 3.5" for perpendicular polarization and 5.7" for parallel. The values agree reasonably well with the values in the measured curves, Figures 24 and 25. These figures also show that the locations of fringe maxima and minima depend on polarization direction.

16

Fringe patterns that are nearly identical for the two polarizations can be produced by equating k_g for the two polarizations. Two methods are available. One is to use distinct thicknesses for the two polarizations. The other is to utilize anisotropic dielectrics. Before discussing these approaches, it is useful to consider how slab interferometers would be installed in a nose cone and how polarization influences the design.

To understand some consequences of polarization for a system, let us consider self-referencing interferometers installed on a nose cone. Figure 26 shows two alternative arrangements.

In Figure 26a, the electric vector is vertical. Consequently the antennas are vertical. At the top of the cross section, the polarization is parallel to the plane of incidence or TM, but on the side the vertical polarization is perpendicular to the plane of incidence or TE. In Figure 26b the field is horizontal at the top but vertical at the side. In all cases the antennas are polarized parallel to the field.

A single antenna polarization, as in Figure 26a, is conventional for seekers in active or semi-active systems. For semi-active or passive systems the polarization of the incident field may change relative to the antenna because the missile or illuminator rolls. However, this source of depolarization is absent from active systems.

Fringe position measurements are possible for perpendicular polarization. Figure 24 shows well defined fringes for perpendicular polarization at 60° incidence, but Figure 25 shows shallow fringes for parallel polarization. For parallel polarization, deep fringes can be formed by increasing dielectric thickness. Figure 27 shows deep fringes for thickness 0.432" at grazing incidence; in contrast, Figure 28 shows no fringes for thickness 0.235". The pattern in Figure 27 resembles the pattern in Figure 29 for perpendicular poarlization at grazing incidence on a slab with thickness 0.23".

17

Another systems approach is to form monopulse patterns with two inter-
ferometers on opposite sides of the nose cone. In this case the fringe
patterns in Figure 25 is preferable to that in Figure 27 (for the
thicker slab) because intensity is higher for the thinner slab.

For an active system the polarization relative to the antennas is fixed,
excluding target depolarization. The configuration in Figure 26b is
suitable.

For a passive, direction finding system the wave polarization can be
general. To handle this case we can use distinct interferometers for
direction finding if space on the vehicle permits. However for a missile
that tracks a target, angles in two planes are needed, and shadowing is
a factor. Therefore an arrangement like that in Figure 20c or 20d is
justified. The wave can be detected with orthogonal antennas in each
slab.

To measure both polarizations with one slab, two orthogonal antennas can
be utilized in one slab. The fringe patterns for the two polarizations
must be similar, in order to place the antennas at approximately similar
intensity levels. Two similar, but displaced fringes are acceptable but
identical fringes are unnecessary because antennas need not be co-located.
However, transmission lines may be simpler and more compact with nearly
identical fringes.

To achieve nearly identical fringes we can utilize anisotropic dielectrics.
Anisotropy can be produced by grooves on a dielectric slab. Figure 30
shows the intensity near a slab with wedge-shaped grooves on one side for ·
the wedge heights parallel to the electric field. A dipole probe scanned

18

a path parallel to the wedges. Figure 31 shows the intensity with the probe center inside the valley between wedges. These figures show that deep fringes can be produced for parallel polarization. Similar fringes were produced for perpendicular polarization. See Figures 32 and 33. The wedge lengths were in the plane of incidence. Additional measurements were made with slabs having parallel dielectric strips. For parallel polarization, the strips produce deep fringes when they are in the plane of incidence but do not when the strips are orthogonal to the plane of incidence.

5.8 Skew Incidence

The analysis and measurements performed so far have considered symmetric incidence as in Figure 34. However in practice waves will arrive with their normals skewed, as in Figure 35. For this more general incidence it is reasonable to expect guided waves of both the TE and TM types. The fringe pattern can be more complicated than the patterns for either the TE or TM mode. The general structure of the field is unknown for skew incidence, but a separation of modes may be useful in a system to simplify angle extraction. In addition to modal separation the fringes may be curved or distorted by refraction of the guided wave. A direct method to simplify angle measurement is to use linearly polarized detectors; that is, to measure only the TE or the TM mode.

To test the field structure for skew incidence, we measured the fringe pattern for skew incidence. The procedure was to place a slab vertically on a turntable and to rotate it to three positions. For each position the transmitting antenna was set at 4 elevation angles. The setup is shown in Figure 36. A dipole probe was scanned near the surface.

Figure 37 shows the locations of the intensity minima. Even to elevation angles of 60° very slight null shift occurs with incidence angle change.

19

To further test the influence of skew incidence we measured minima positions for a slab with a circular profile on one end as in Figure 38. Here we see more influence of incidence angle. The rectangular profile seems superior in that fringe behavior remains relatively fixed for changes in incidence angle below 60°; at higher angles the circular seems better.

5.9 Angular Accuracy

The accuracy in measuring incidence angle is significant for applications. Precise, quantitative statements depend on the instrumentation so a general evaluation is beyond the scope of this project. However we have obtained data for two kinds of systems.

We measured the angle of arrival by measuring two values of fringe spacing. The accuracy was 0.18°, which is very similar to boresight error of conventional radomes. Of course boresight error rates of change are significant for guidance, but detailed measurements were not made.

The second example is the monopulse pattern in Figure 18. We expect accuracy comparable to that of body-fixed monopulse systems.

5.10 Metallic Surfaces

The dielectric slabs will be surrounded by metallic aircraft structure.* The metal can be useful in reducing sidelobe levels, as shown in Section 2. However the metal can also inhibit guided wave excitation if it is at the leading edge. Therefore the dielectric will be tapered in thickness and the sensor will be placed on the slab where excitation is adequate.

*Although the slabs might be utilized like blade antennas in some cases, missile noses and aircraft skins are likely locations. For extremely high missile temperatures, dielectrics may be too weak so some metallic surroundings must be considered.

6. REFERENCES

1. R. F. Harrington, <u>Time-Harmonic Electromagnetic Fields</u>,
    McGraw Hill pp

2. G. Tricoles, E. L. Rope, and R. A. Hayward, "Wave Propagation
    Through Hollow Dielectric Shells", General Dynamics Electronics
    Division Report R77-092-5, Nov. 1978, Final Report for Contract
    N00019-77-C-0303; Section 5.

3. G. Tricoles and E. L. Rope, "Scattering of Microwaves by
    Dielectric Slabs and Hollow Dielectric Wedges", Jour. Opt. Soc.
    Am., Vol. 55, pp 1479-1498 (1965).

4. See Reference 2.

5. G. Tricoles, E. L. Rope and R. A. Hayward, "Wave Propagation Through
    Axially Symmetric Dielectric Shells", General Dynamics Electronics
    Division Report R80-008, February 1980, Final Report for Contract
    N00019-78-C-0594.
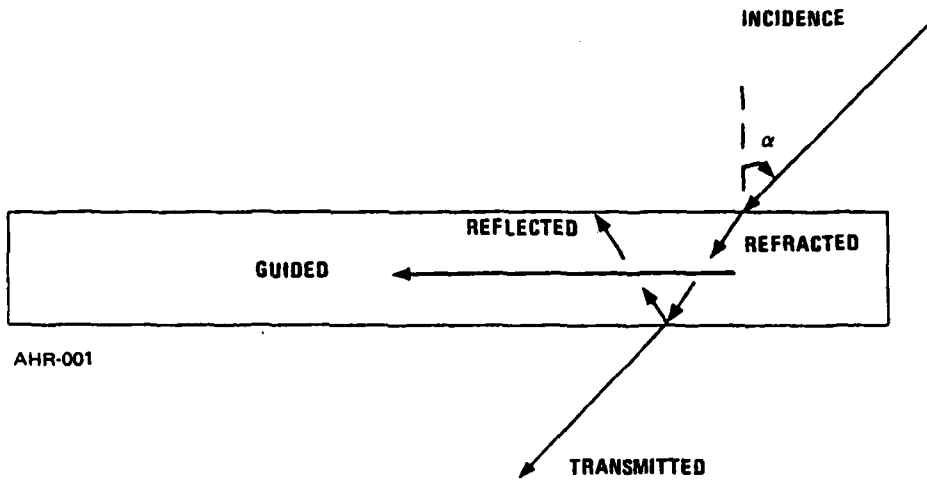
AHR-001

Figure 1.   Waves On A Slab
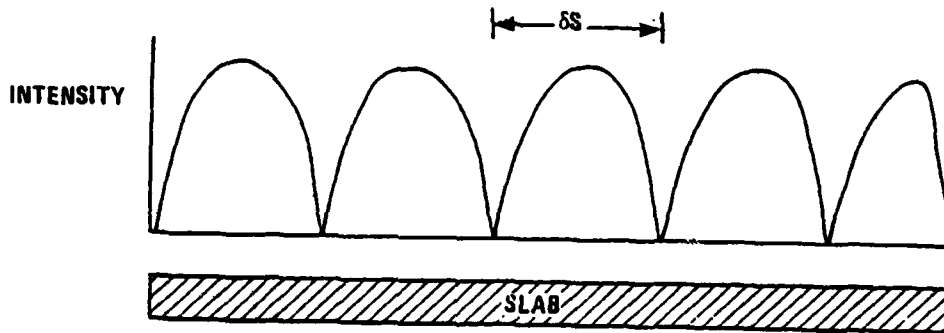
AHR-002

Figure 2.   Intensity Fringes Are Formed Near A Slab
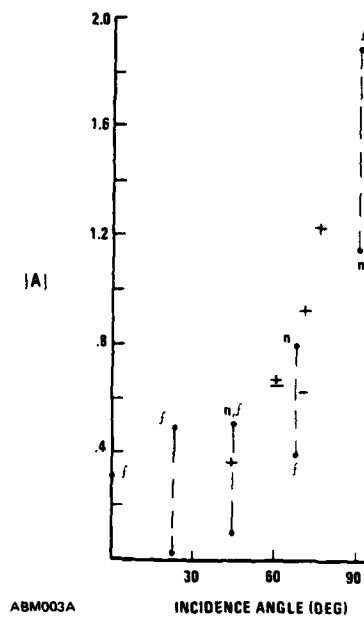
Figure 3. Amplitude of Guided Wave in Slab. Measured at maximum of fringe pattern $(+)_i$ measured at minimum $(-)$; with correction for exportential decay. Computed by extension of moment method $(.)$, where n denotes values at edge nearer source, and f denotes opposite edge. Slab thickness 0.63 cm, wavelengths 3.18 cm, dielectric constant 2.6.

23
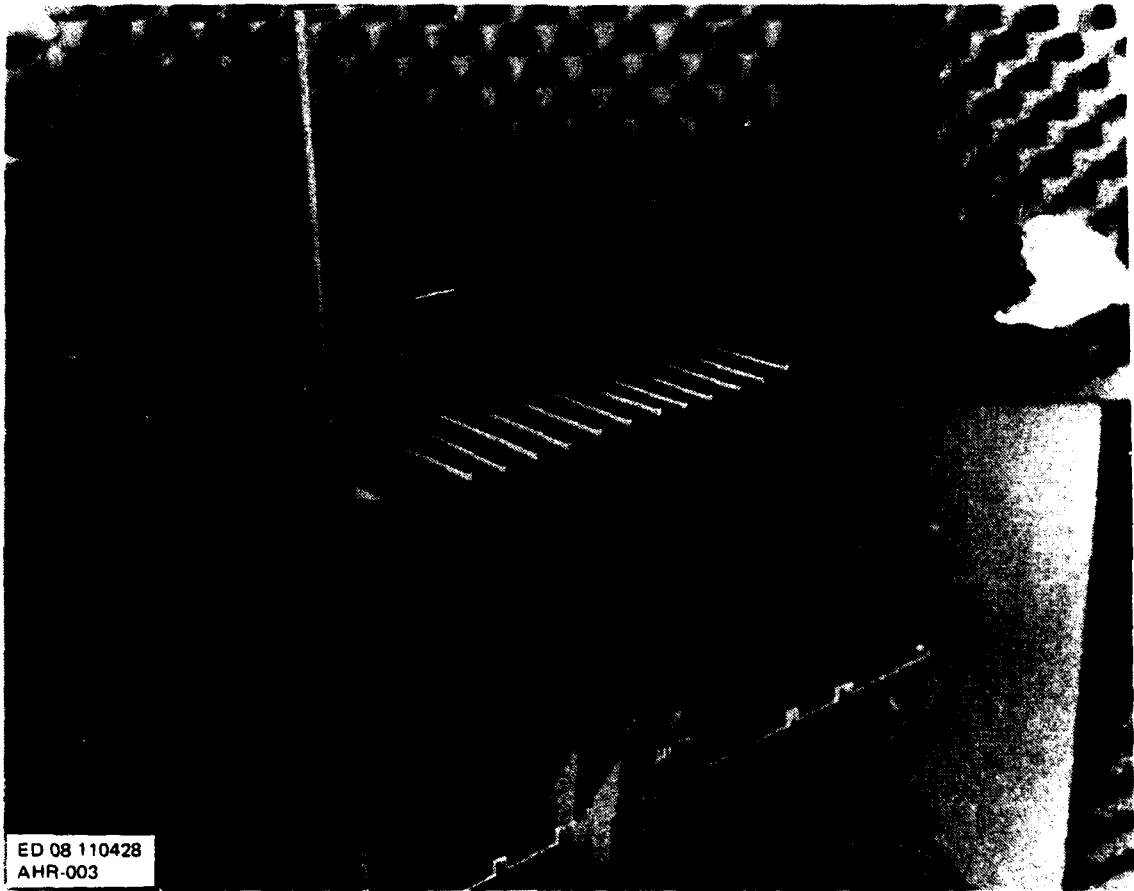
Figure 4. Sampling Array and Dielectric Slab
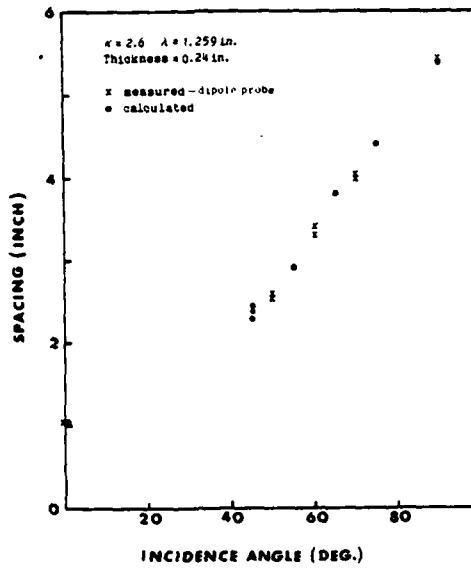
Figure 5.   Spacing of Interference Minima.   The calculations were done with the
Moment Method.   Measurements were made with a dipole antenna scanned
paralled to the slab, at .05" distance.   Polarization was perpendicular.
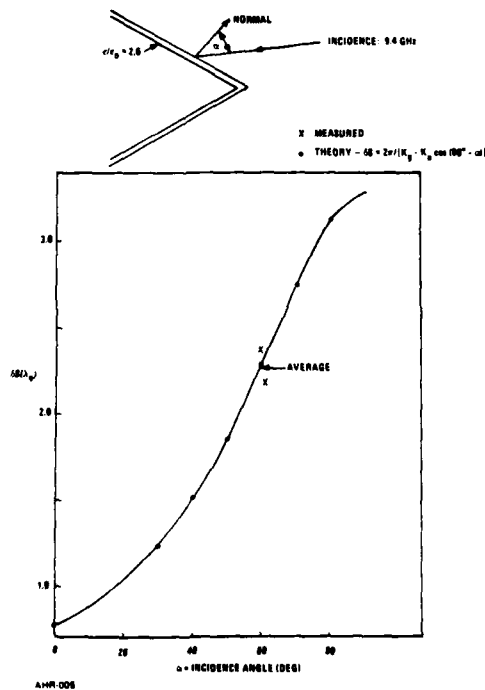
Figure 6.   Spacing Variation with Incidence Angle

25
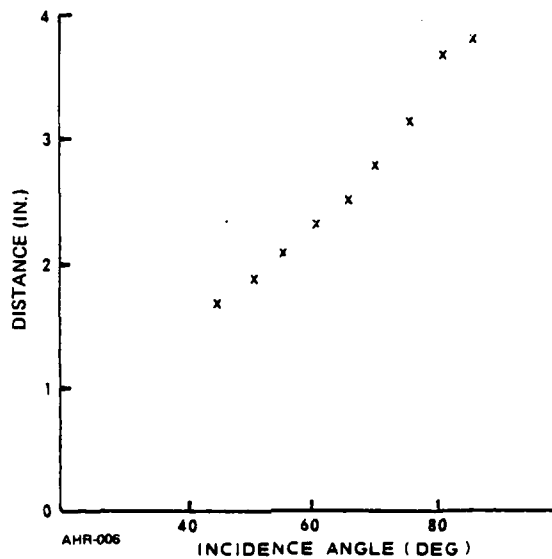
Figure 7. Distance, Panel Edge to First Null for 0.245 In. X 18.0 In. Panel
with Beveled Rear Edge. $\kappa = 2.6$ $\lambda_0 = 1.259$ In. Measured with probe
to Panel Separation 0.05 In.
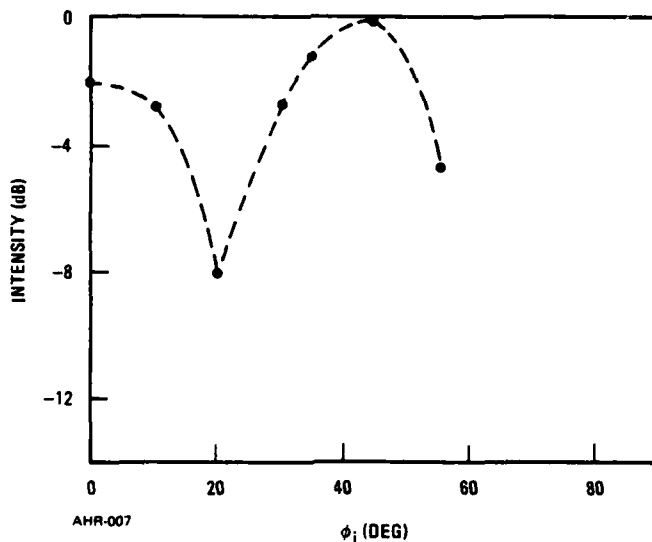
Figure 8. Intensity produced by summing E^T at x = 2.0" and 2.5" in dielectric
slab with thickness 0.25" dielectric constant 2.6, for frequency
9.4 GHz.

26
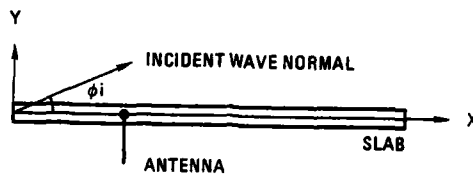
AHR-008

Figure 9. An Elementary *Self-Referencing Interferometer* consisting of a dielectric slab with an embedded antenna
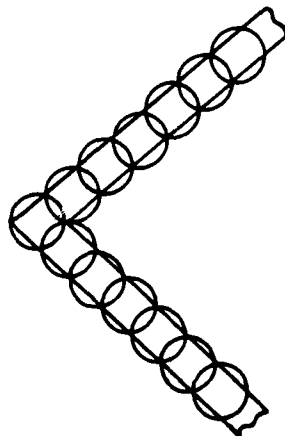
GE001

Figure 10. Subdivision of Wedge into Parallel Cylinders.
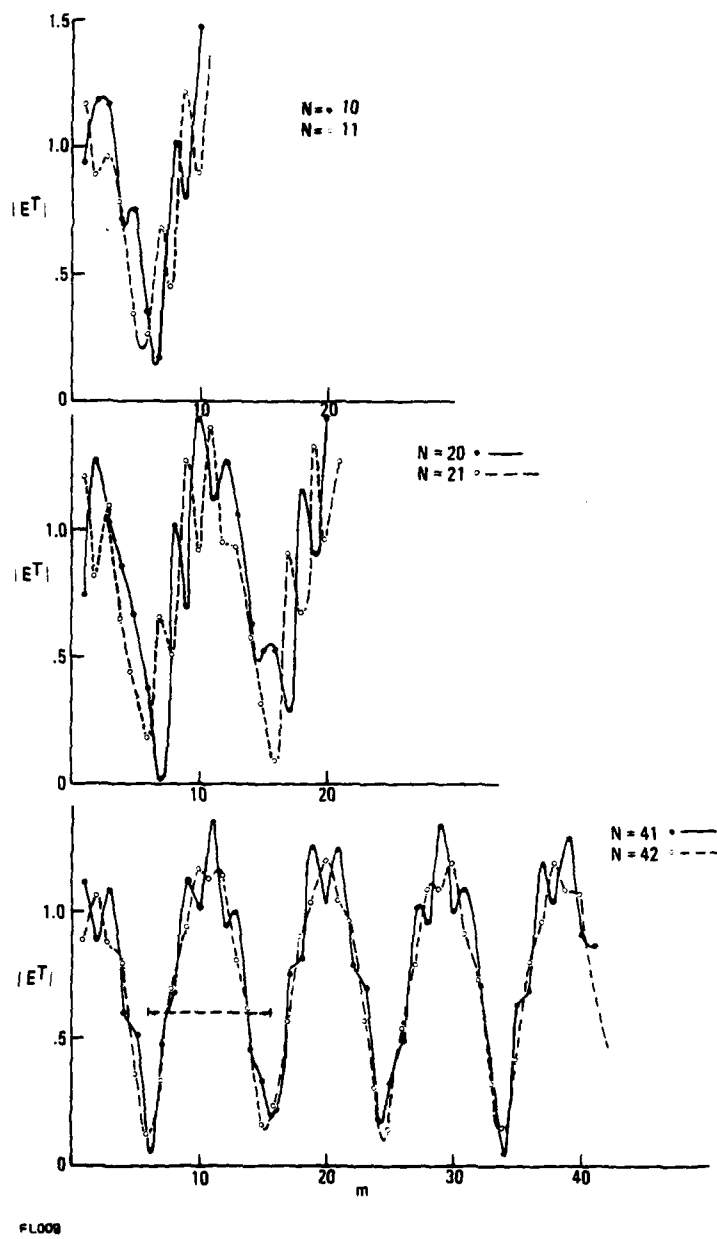
Figure 11. Total Field Magnitude Inside Dielectric Slabs for 45°, $\lambda = 1.259$ in. Computed for a = 0.143 in., $\rho = 0.250$ in. The arrows show theoretical fringe spacings for guided waves.

28
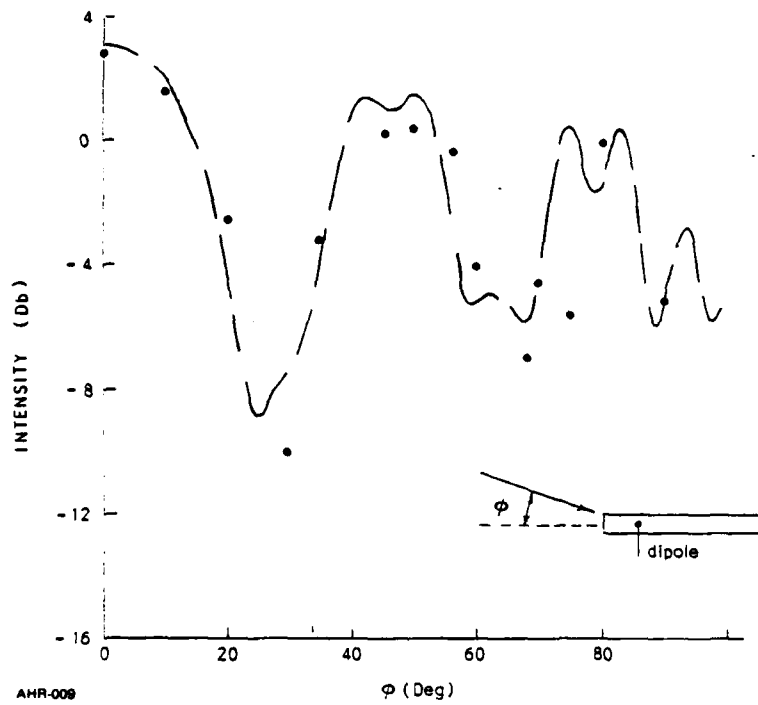
Figure 12. Intensity Received by Dipole in Slab. Frequency: 9.400 GHz
Measured (- -). Calculated (.). Dielectric Constant 2.6.
Thickness: 0.25 in. Dipole 2.4 inch from illuminated edge.

Figure 13. Intensity for Two Dipoles in a Slab
The curve was measured; (·) indicates computations.

30
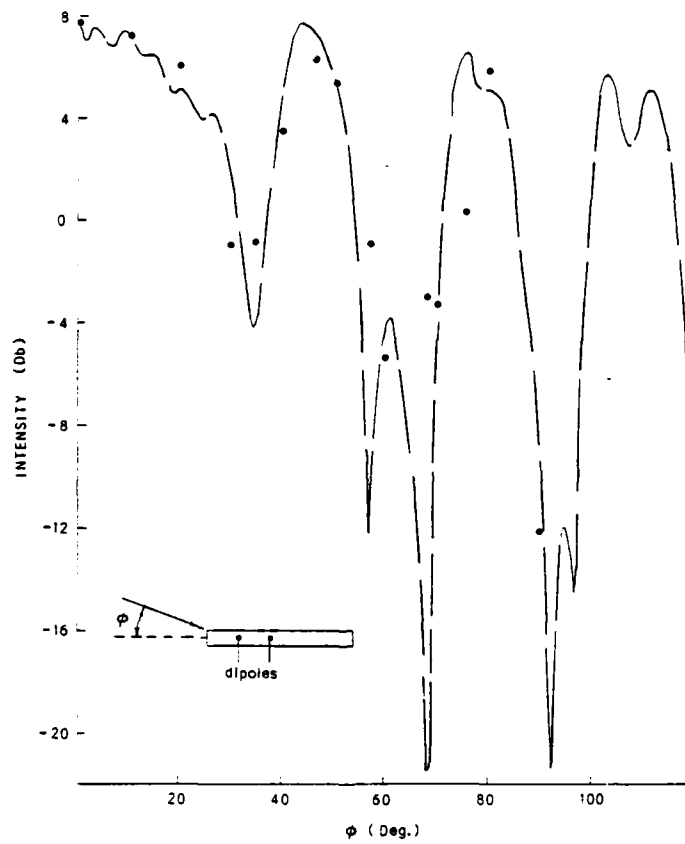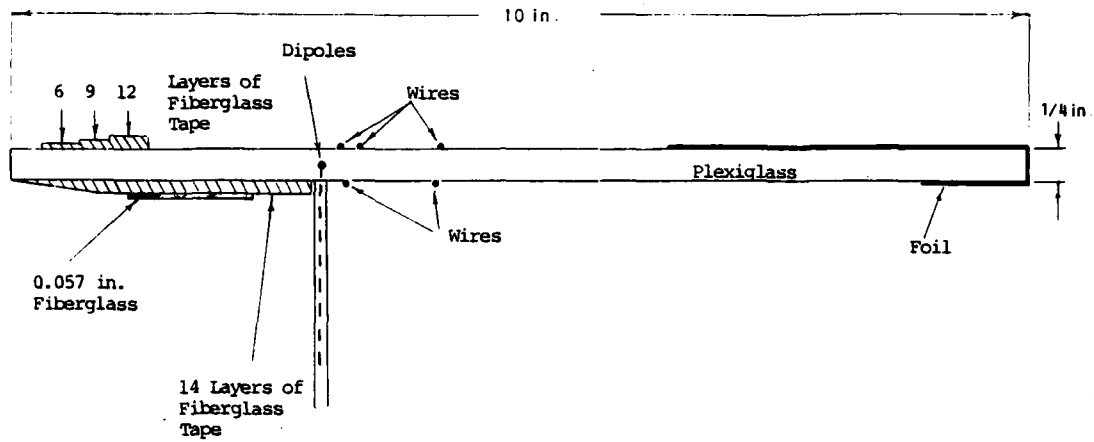
Figure 14.   Antennas Embedded in a Non-Uniformly Thick Slab
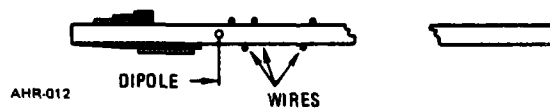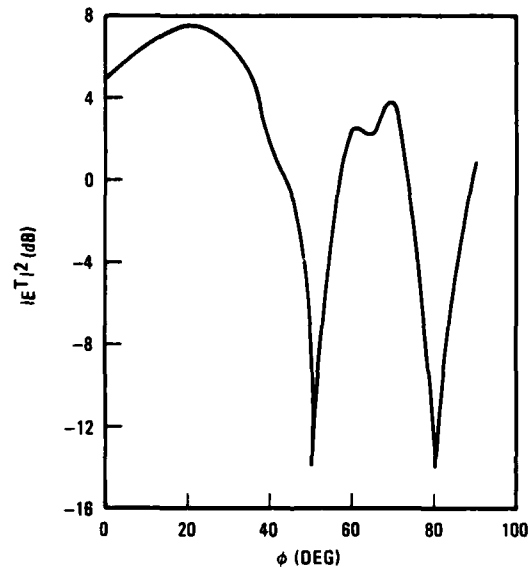
Figure 15.   Computed Field in a Quarter Inch Tapered Slab with Wires and
Dipole, at Location of Dipole

31
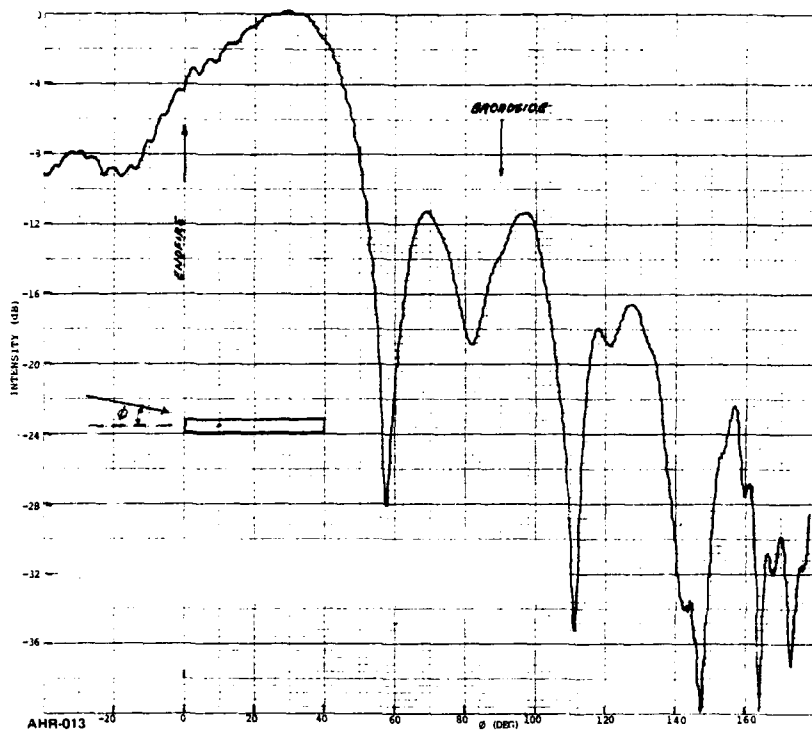
Figure 16.   Intensity for two, colinear dipoles in non-uniform slab.
             Frequency 9.4 GHz.
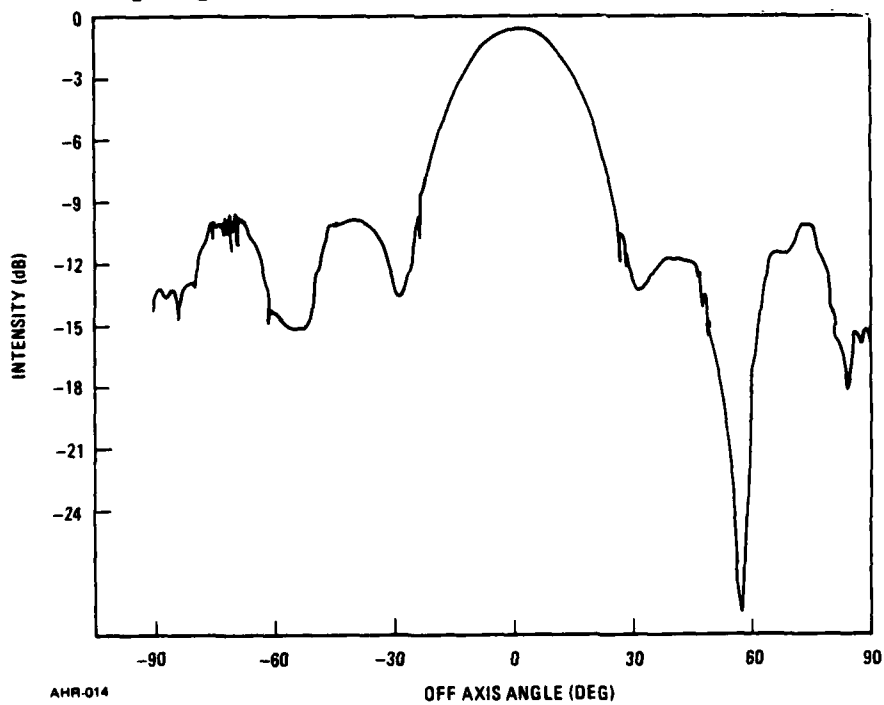
Figure 17.   Sum mode pattern formed by two interferometers.   Each slab had
             tapered thickness and one dipole on its surface.
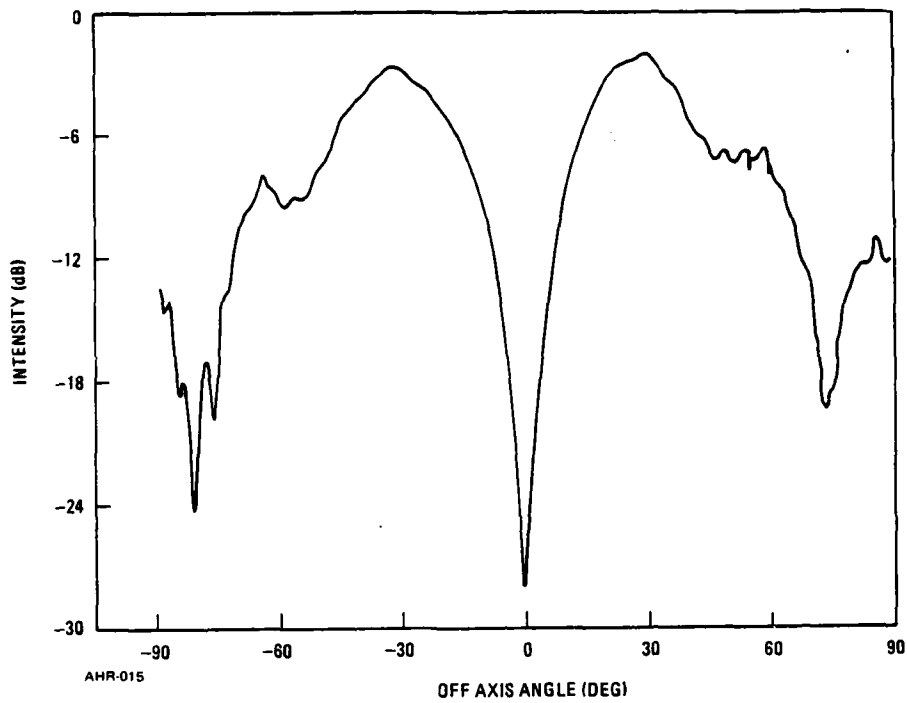
Figure 18. Difference mode pattern for two interferometers formed into a wedge
            Frequency 9.4 GHz.
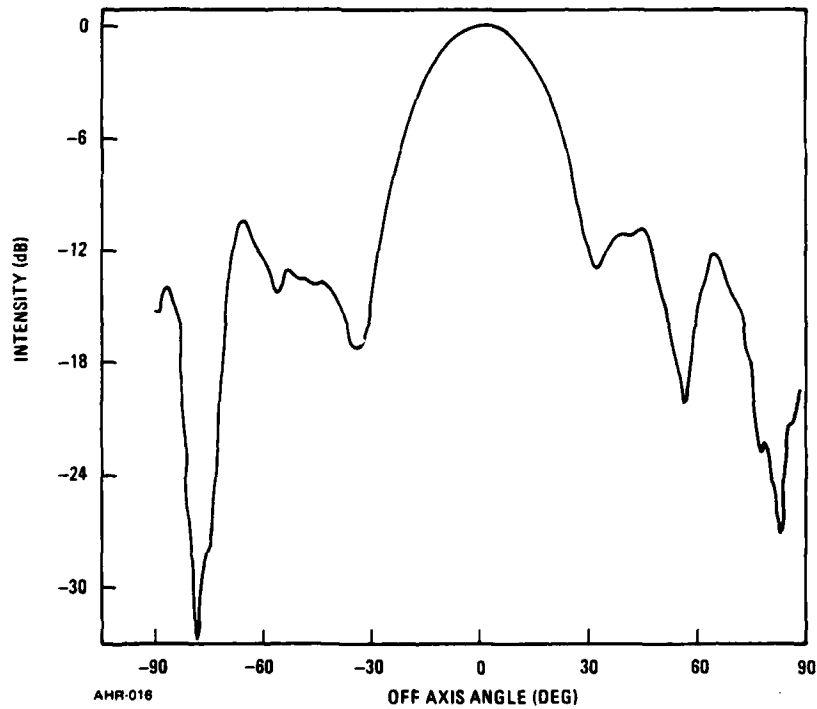
Figure 19. Sum mode pattern formed by two interferometers formed into a wedge
            Each slab had tapered thickness and had two colinear dipoles on its
            surface
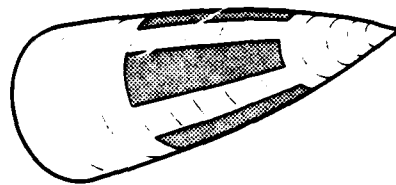
(a) INTERFEROMETERS ON MISSILE NOSE
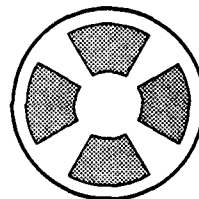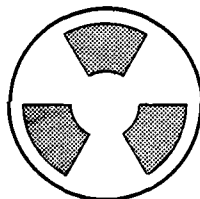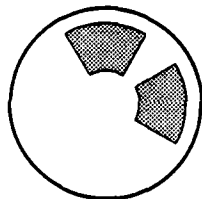
(b) TWO INTERFEROMETERS   (c) THREE INTERFEROMETERS   (d) FOUR INTERFEROMETERS

AHR-017

Figure 20. Installations of Self-Referencing Interferometers on Missile Nose.
The interferometers in (b) can be diametrically opposite for a
rolling airframe.

34
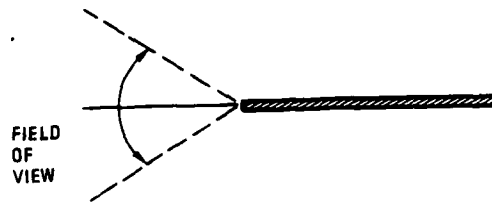
Figure 21. Definition of Field of View
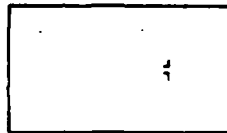
(a) SLAB WITH ONE ANTENNA
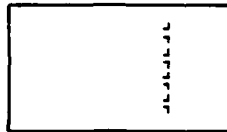
(b) SLAB WITH FOUR COLINEAR ANTENNAS
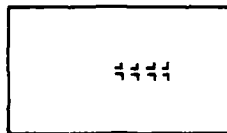
(c) SLAB WITH FOUR PARALLEL ANTENNAS

AHR-019

Figure 22. Alternative Configurations of Sensors

35

E •——► PROPAGATION DIRECTION

(a) PERPENDICULAR POLARIZATION (RELATIVE TO INCLINE PLANE); THIS IS TE CASE

E ↕ ——► PROPAGATION DIRECTION

(b) PARALLEL POLARIZATION (RELATIVE TO INCLINE PLANE); THIS IS TM CASE
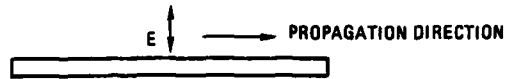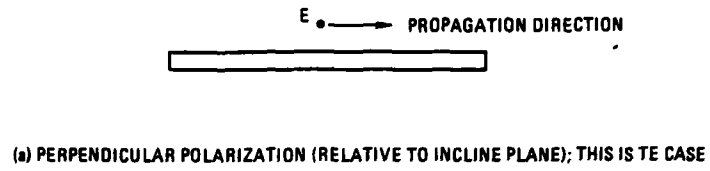
AHR-020

Figure 23.   Terminology for Polarization

NO PANEL

4 dB

LEADING EDGE

|←— 1 INCH —→|
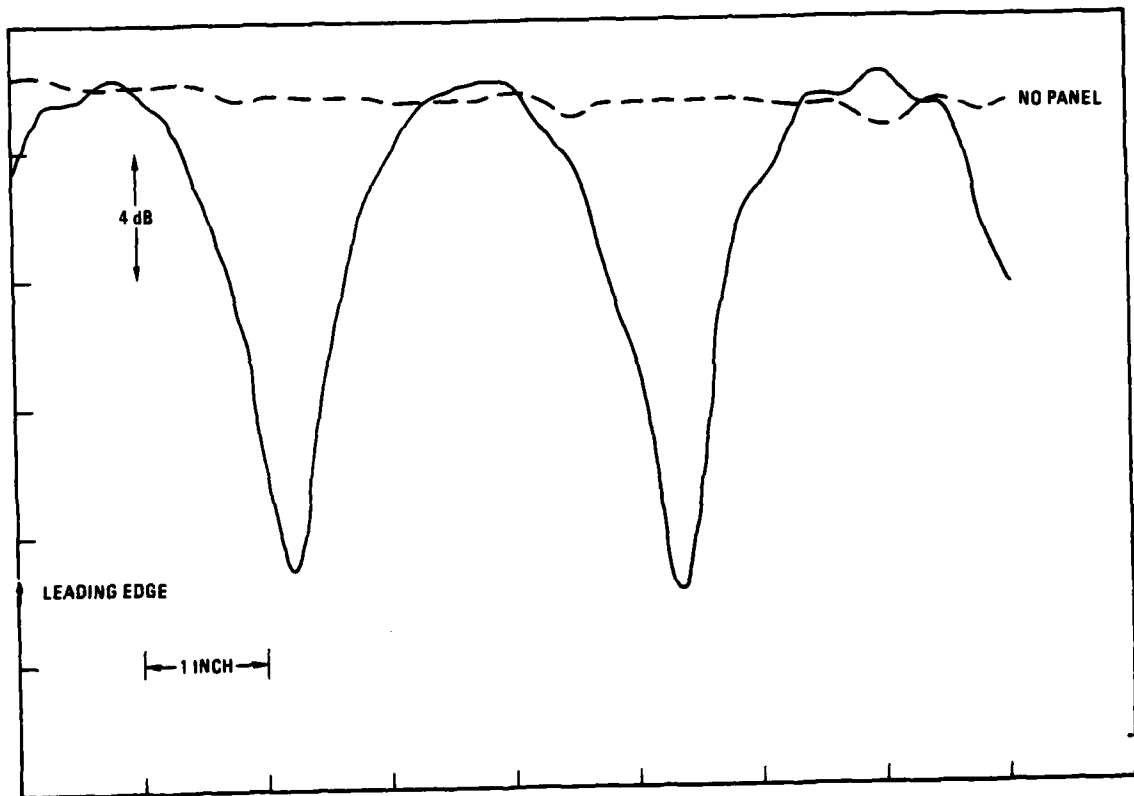
AHR-021

Figure 24.   Intensity near slab for Perpendicular Polarization.   Thickness
0.25", Frequency 9.4 GHz, Incidence Angle 60°

36
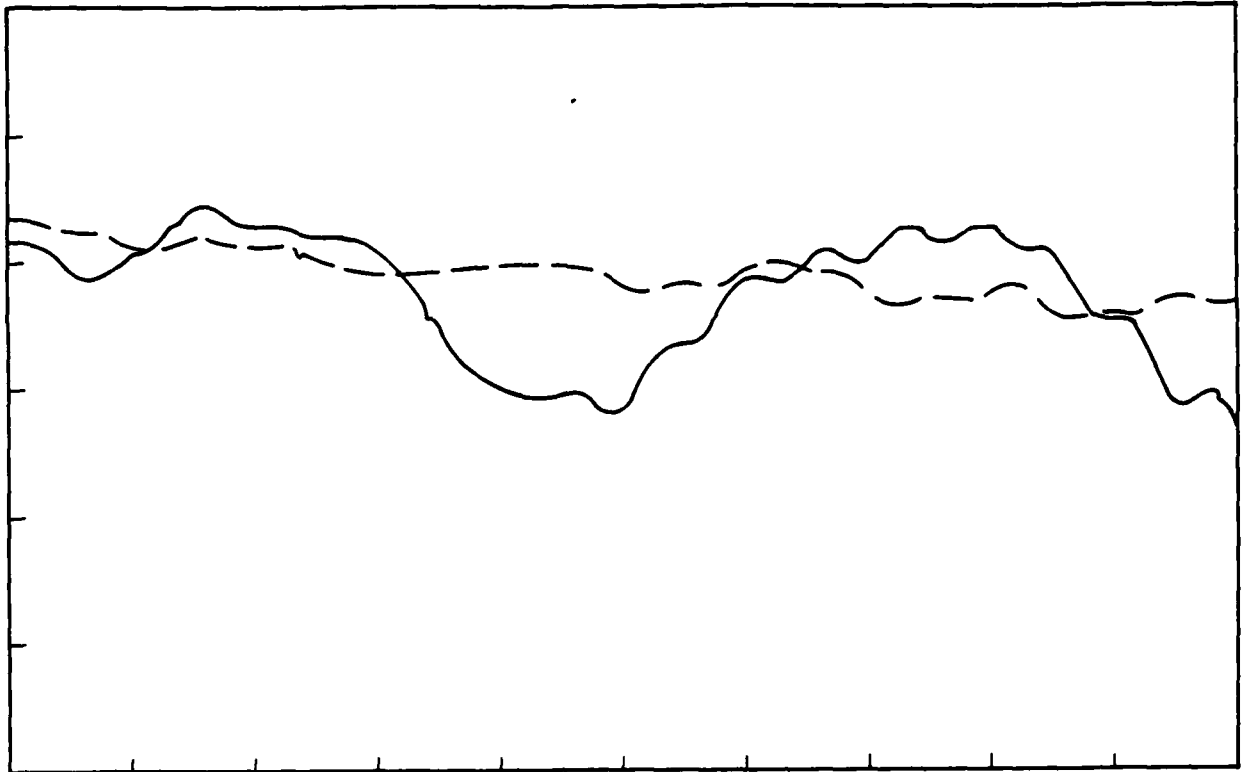
AHR-022

Figure 25.   Intensity Near Slab for Parallel Polarization
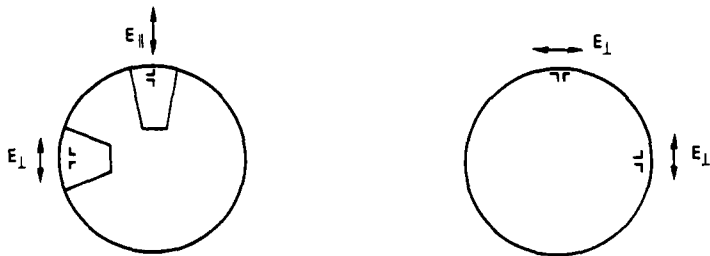
(a) SINGLE SPATIAL ORIENTATION OF E
GIVES POLARIZATION VARYING BETWEEN
PARALLEL AND PERPENDICULAR

AHR-023A

(b) TWO SPATIAL ORIENTATIONS OF E

Figure 26.   Polarization Orientation on a Cone.   The figure presents axial views.
E represents the electric field.   The circles represent cross sections
of an airplane.   Antennas are represented by the symbol (⊣⊢).

37
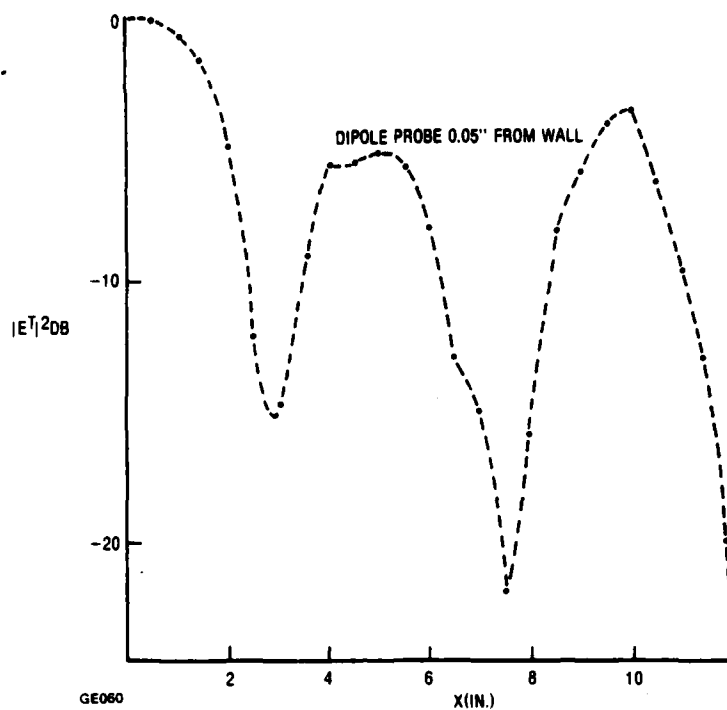
Figure 27.   Measured Power Transmittance Near 0.432 in.   Thick Dielectric Slab
for Grazing Incidence, Polarization Parallel
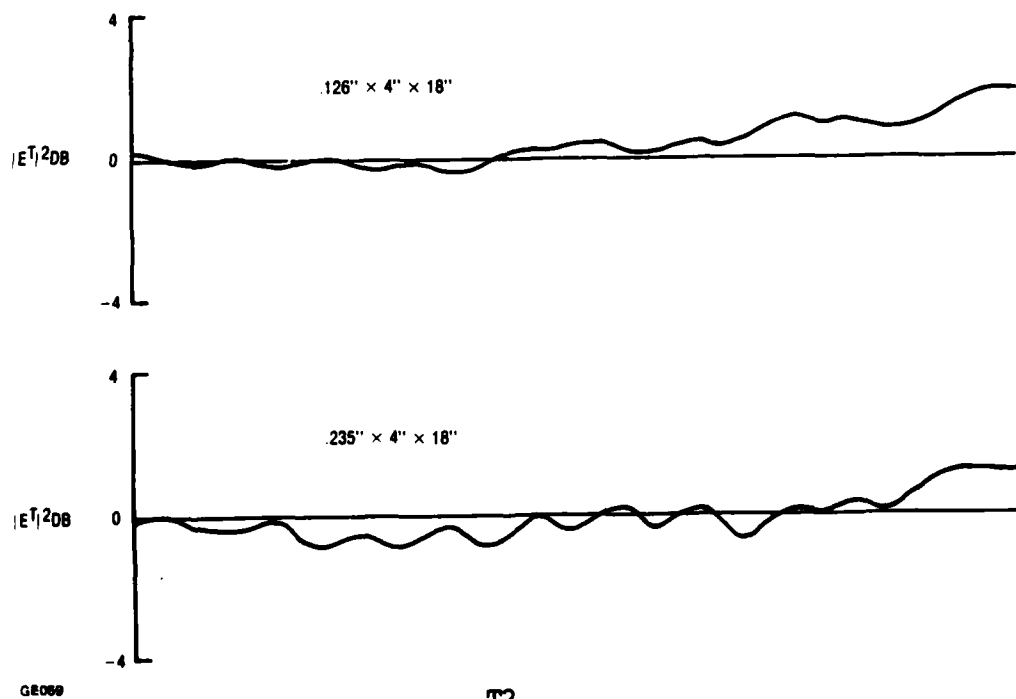
Figure 28.   Measured $|E^T|^2$ For Parallel Polarization

Y = .525 INCH

$|E^T|^2$ dB

0

-4

-8

-12

-16

-20

-24

-2   0   2   4   6   8   10

X (INCH)

FL024
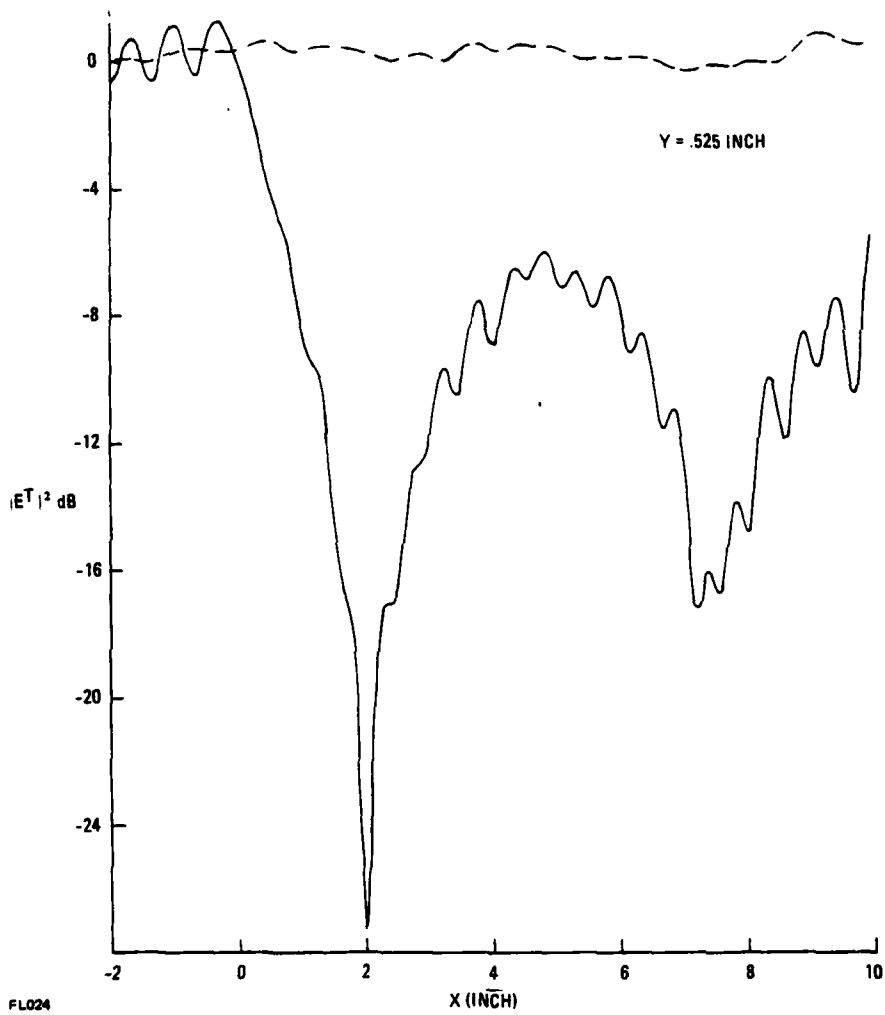
Figure 29.   Measured Intensity Near Slab at Y = 0.525 in.   The dashed curve is
the level without slab thickness .23 in.

4dB

NO SLAB

PROBE

1"
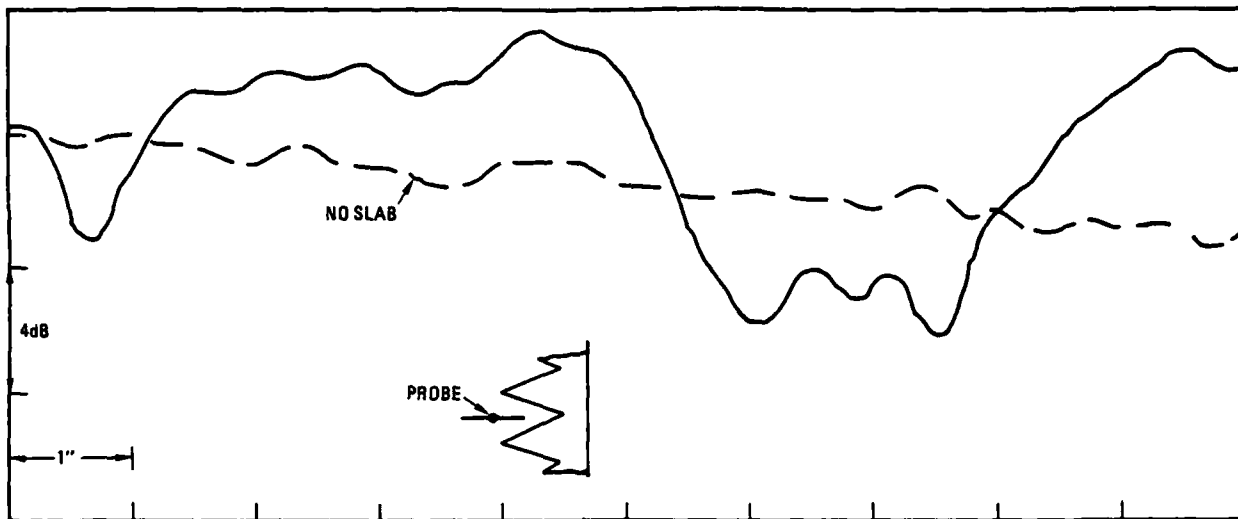
AHR-024

Figure 30.   Intensity Near Grooved Slab for Horizontal Polarization.   Probe
Center 0.1" Outside Wedge Tips.   Incide Angle 60°.

4dB

PROBE

1"
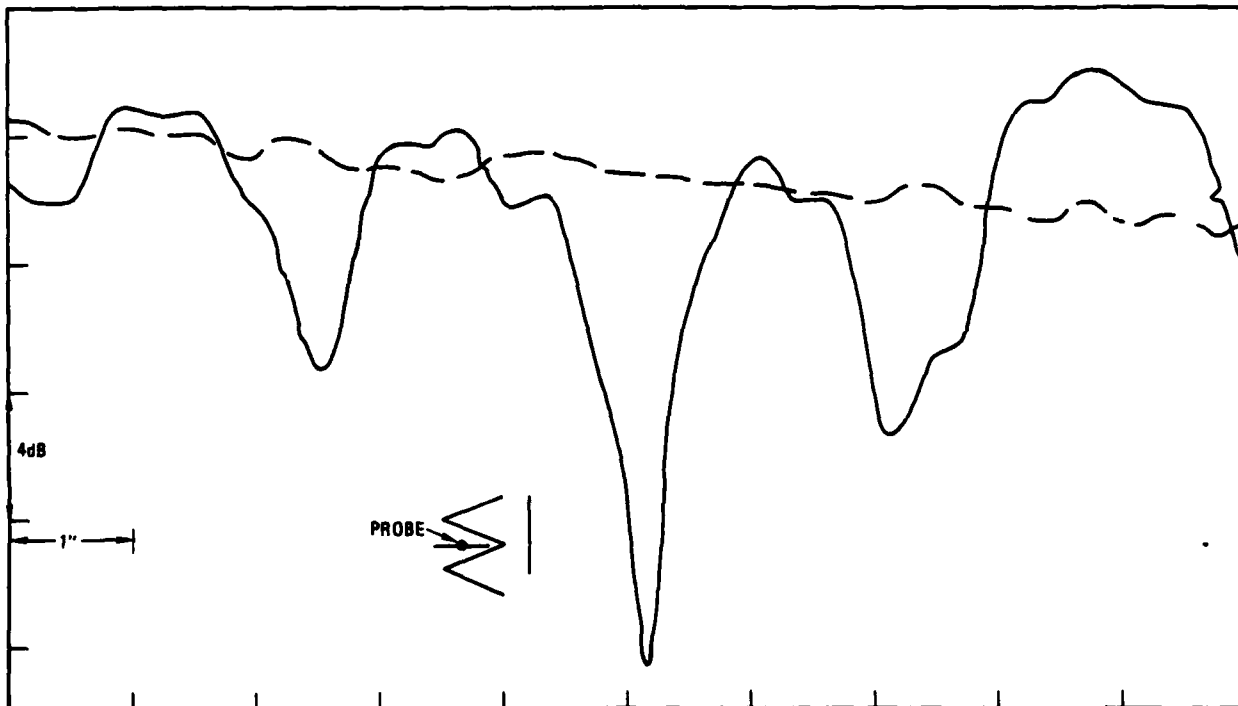
AHR-025   Figure 31.   As in Figure 30 but with Probe moved closer to slab

40
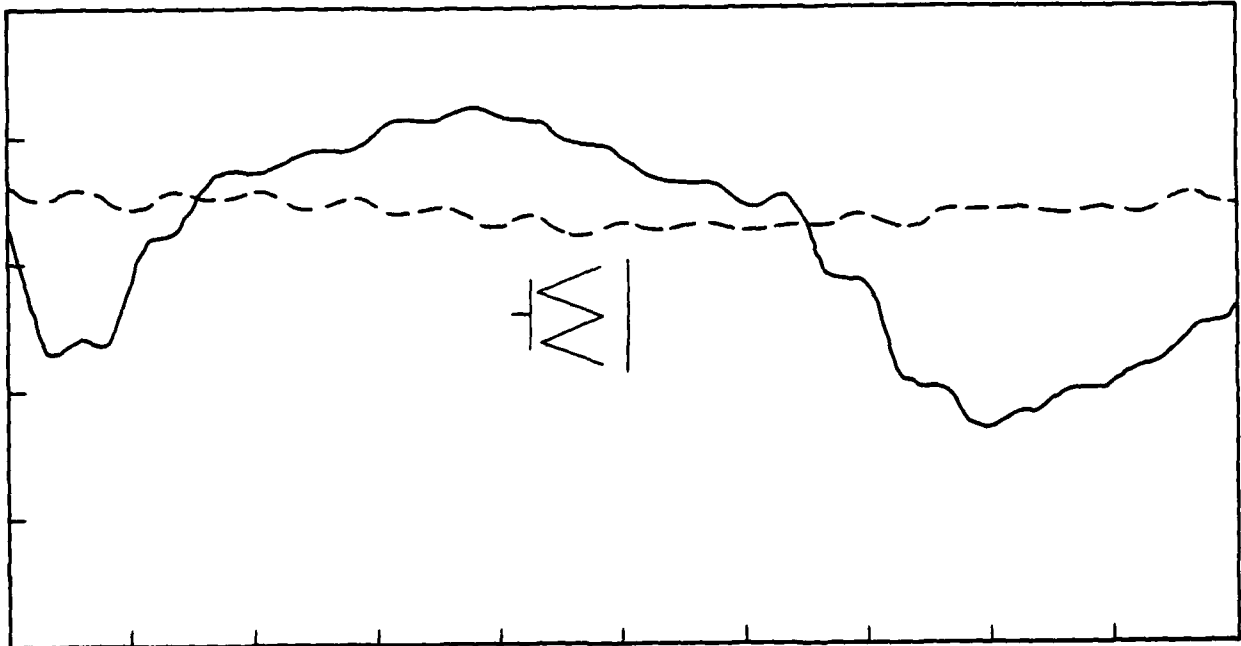
AHR-026

Figure 32.   Intensity Near Grooved Slab for Perpendicular Polarization
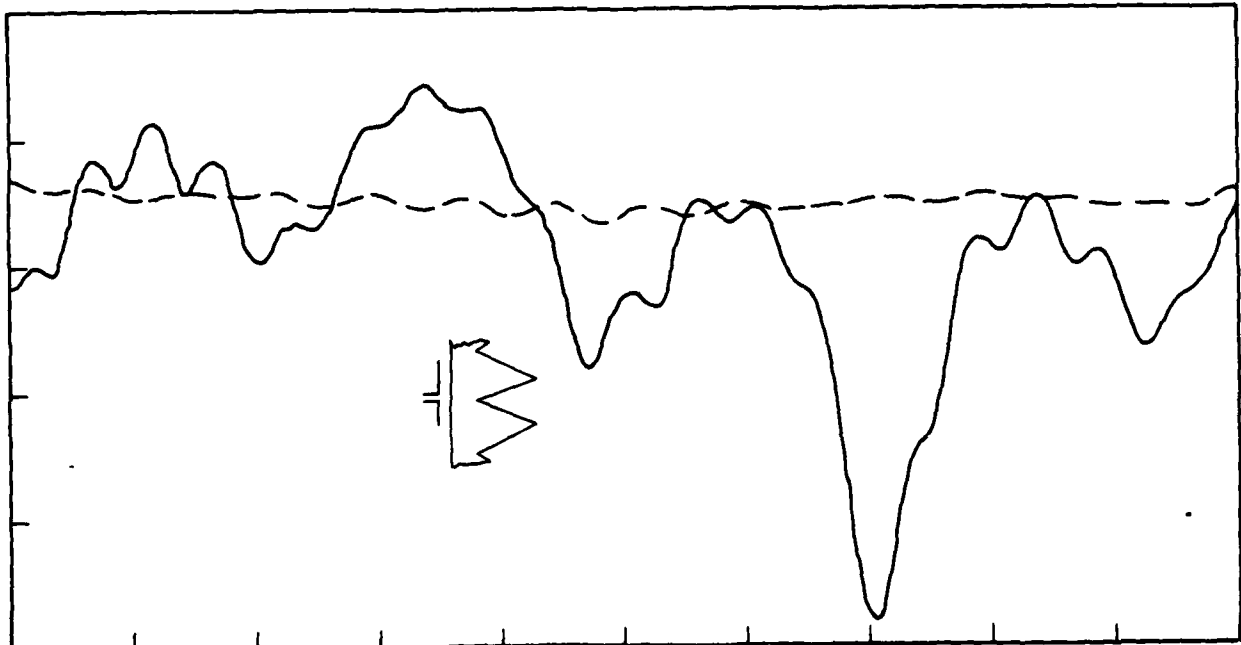
AHR-027

Figure 33.   As in Figure 32 but for Probe on Flat Side

41

AHR-028
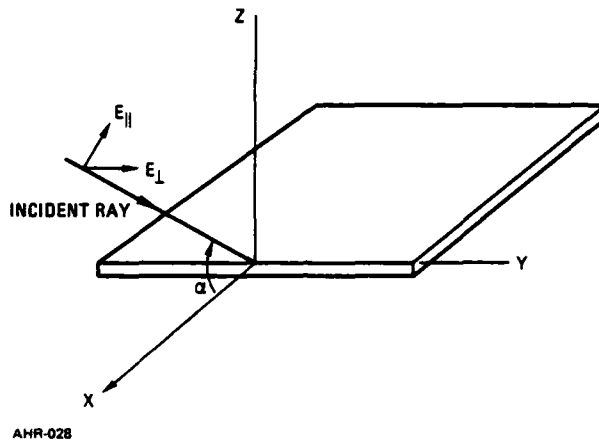
Figure 34.   Plane Wave Symmetrically Incident on Dielectric Slab

AHR-029
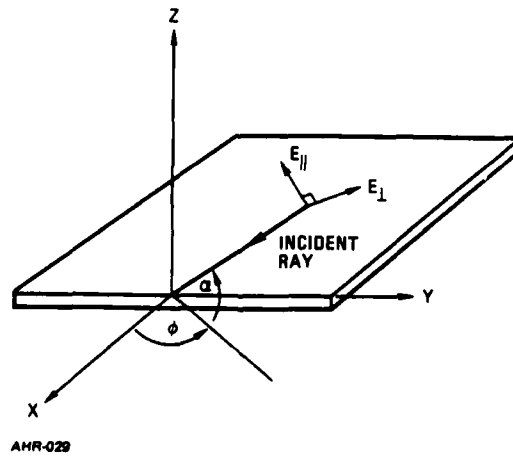
Figure 35.   Skew Incidence

TRANSMITTER
ANTENNA

AZIMUTH ROTATION

PROBE

ELEVATION ANGLE

TURNTABLE

AHR-030
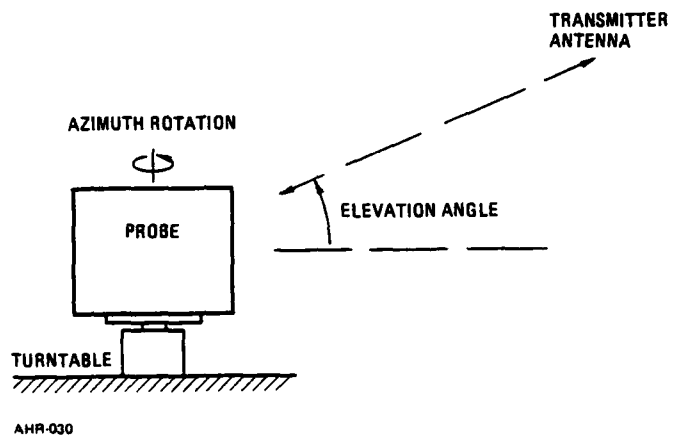
Figure 36. Probing Setup for Skew Incidence

43
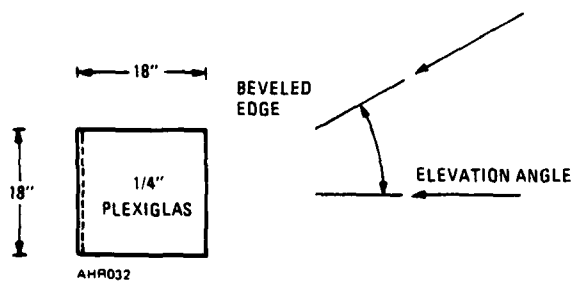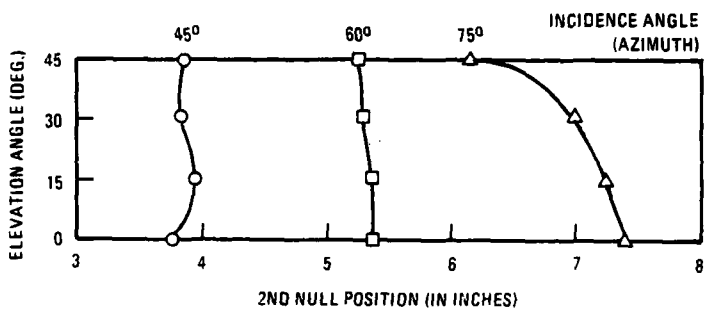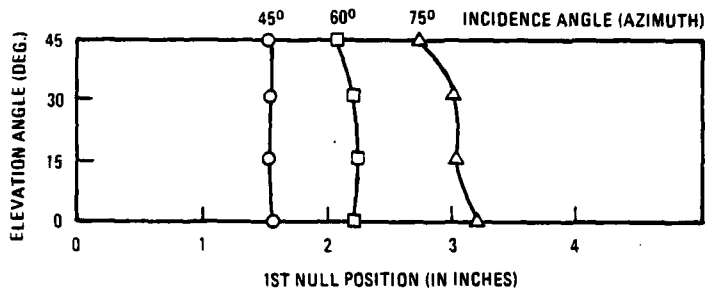
Figure 37. Minima Positions for Square Slab
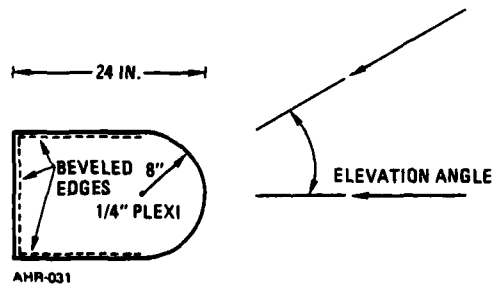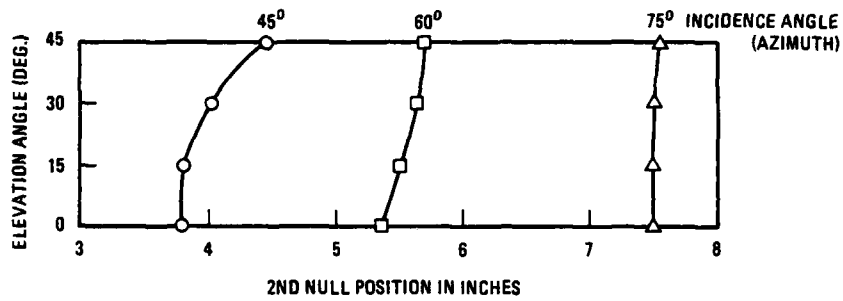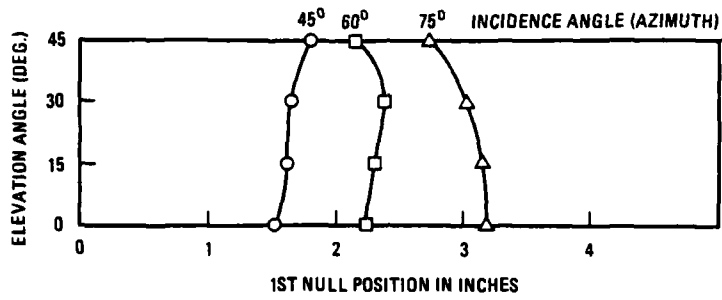
Figure 38.   Minima Position for Slab with Circular Forward Part

45